Optimizing the Topology of Tendon-Driven Fingers: Rationale, Predictions and Implementation

Joshua M. Inouye, Jason J. Kutch, and Francisco J. Valero-Cuevas, *IEEE Member*

Abstract

Tendon-driven mechanisms in general, and tendon-driven fingers in particular, are ubiquitous in nature, and are an important class of bio-inspired mechatronic systems. However, the mechanical complexity of tendon-driven systems has hindered our understanding of biological systems, and the optimization of the design, performance, control, and construction of mechatronic systems. Here we apply our recently-developed analytical approach to tendon-driven systems [1] to describe a novel, systematic approach to analyze and optimize the routing of tendons for force-production capabilities of a reconfigurable 3D tendon-driven finger. Our results show that these capabilities could be increased by up to 277% by rerouting tendons, and up to 82% by changing specific pulley sizes for specific routings. In addition, we validate these large gains in performance experimentally. The experimental results for 6 implemented tendon routings correlated very highly with theoretical predictions with an R^2 value of 0.987, and the average effect of unmodeled friction decreased performance an average of 12%. We not only show that, as expected, functional performance can be highly sensitive to tendon routing and pulley size, but also that informed design of fingers with fewer tendons can exceed the performance of some fingers with more tendons. This now enables the systematic simplification and/or optimization of the design and construction of novel robotic/prosthetic fingers. Lastly, this design and analysis approach can now be used to model complex biological systems such as the human hand to understand the synergistic nature of anatomical structure and neural control.

Index Terms

biologically-inspired robots, mechanism design

I. Glossary

- Tendon-driven system: any mechanical system that is actuated (either actively or passively) with tendons that can only pull and not push (e.g., wires, cables, strings, etc.).
- Tendon routing: the configuration in which the tendons are arranged in a tendon-driven system.
- Feasible force set: the convex set in endpoint force space (normally 2-D or 3-D) that encloses all achievable force vectors based on the parameters of a tendon-driven manipulator.
- Moment arm matrix: a matrix that contains information about all of the moment arms in a tendon-driven manipulator. Each row corresponds to a joint and each column to a specific tendon. The entries are the values of the moment arms.
- Jacobian: a matrix that transforms joint angle velocities to manipulator endpoint velocities.
- Minkowski sum: in this context, it all possible positive or zero combinations of the collection of basis vectors for the tendons. Stated another way, it contains all possibilities of full or zero activation for all of the tendons.
- Posture: a set of joint angles.
- Maximum isotropic value (MIV): the greatest possible force that a robotic finger or manipulator can exert in all directions (i.e., isotropically).

This material is based upon work supported by NSF Grant 0836042, NIDRR Grant 84-133E2008-8, and NIH Grant AR050520 and Grant AR052345 to F. J. Valero-Cuevas.

J. Inouye is with the Department of Biomedical Engineering, University of Southern California, CA, 90089 USA. e-mail: jinouye@usc.edu.

J. Kutch is with the Division of Biokinesiology and Physical Therapy, University of Southern California, CA, 90089 USA. e-mail: kutch@usc.edu.

Corresponding author: F. J. Valero-Cuevas is with the Department of Biomedical Engineering & the Division of Biokinesiology and Physical Therapy, University of Southern California. e-mail: valero@usc.edu

II. Introduction

BIO-INSPIRED robotic hands employ multiple robotic fingers for dexterous grasping and manipulation tasks [2]–[13]. Bio-inspiration can refer to their tendon-driven nature, but also the asymmetry of the routings, the variation in moment arm sizes, and the non-uniform distribution of maximal tendon tensions. Robotic finger kinematics may be anthropomorphic or they may be less complex to simplify the construction and control of the fingers. Moreover, two fundamental classes of actuation are typically used: i) those that use remote actuation (e.g., motors outside the fingers which actuate tendons, cables, or gears) and ii) those that use internal actuation (e.g., motors inside the fingers). Tendon-driven limbs and fingers are ubiquitous in vertebrates, and such bio-inspired tendon-driven actuation has proven engineering design advantages such as light weight, low inertia, small size, backdrivability, and design flexibility [14]. However, the mechanical complexity of tendon-driven systems (e.g., the large number of design parameters) has precluded the development of modeling, design, and analysis tools to optimize their performance, control, and construction. In this paper, we analyze, optimize, and test alternative implementations of a 3D tendon-driven robotic finger. We validate this approach with physical hardware implementations from the functional perspective of maximizing the set of feasible endpoint static forces.

Many considerations go into the design of robotic fingers and hands, such as force and velocity production, control, ease of construction, design simplicity, and cost. Adequate force-production capabilities are a necessary element of the multidimensional design puzzle: according to Firmani,"The knowledge of maximum twist and wrench capabilities is an important tool for achieving the optimum design of manipulators" [15]. In fact, if a finger cannot produce sufficient endpoint force while meeting other critical design requirements such as size and number of motors (for example in space, hazardous or surgical applications), then the mechatronic system is useless regardless of the attributes of the controller or ease of manufacturing. Therefore, as a demonstration of our novel modeling, analysis and optimization approach, we concentrate on the kinetostatic (endpoint force-production) capabilities for robotic fingers.

Several studies have analyzed the kinetostatic performance of tendon-driven and torque-driven manipulators [15]–[23] (determining the kinetostatic capabilities given design parameters), and several others have addressed their optimization or synthesis (specifying the design parameters given desired capabilities) [24]–[32]. These studies are based on mathematical theory. The fabrication of robotic fingers has been widely accomplished for robotic hands [2]–[13]. Experimental testing of kinetostatic performance can be found in the biomechanics literature [33], [34], but these do not implement a system whose parameters can be altered. We combine these three areas of *theory, fabrication, and testing* to optimize and validate hardware implementations of alternative robotic finger designs.

III. Nuances of Biological and Engineering Systems that are Tendon-Driven

Understanding the mechanical properties of tendon-driven plants is critical to understanding the actual problem confronting both brain-body dynamics and the plant-controller engineering design problem. Elsewhere we have shown the importance of understanding the nuances of tendon-driven systems that cannot be understood when applying the common torque-driven mathematical approach to the actuation of serial kinematic chains (i.e., limbs [35]). However, a brief summary is warranted because the present work is motivated by the need to understand well (i) the consequences of alternative tendon routings (i.e., system topologies) and their optimization; and (ii) the need to validate the analytical and computational approaches we have developed and promoted in prior work.

The nuances of tendon-driven systems include:

- *Topology matters*: When thinking of the structure and function of anatomical and engineering systems, it is important to distinguish between the topology of the system and its specific parameter values [36]. The topology consists of the type and connectivity of elements of any particular systems, which in this case include the number and type of kinematics degrees of freedom, and the way in which tendons cross and actuate joints. The specific parameters then include the actual number of limb segments, degrees of freedom, the kinematic connectivity across limb segments and the specifics of how many tendons there are, which kinematic degrees of freedom they cross and actuate, and the moment arm at each degree of freedom (assuming only rotational degrees of freedom). We have shown, for example, that apparently similar topologies can have very different mechanical capabilities [36], and that some topologies can be used to satisfy various functional goals [37]. Therefore the topology and parameters values of a tendon-driven system must be considered carefully.

- *Agonists, antagonists and co-contraction*: The perspective and language that emerges from analyzing single joint systems such as the elbow or knee are very often not valid in the case of multi-articular, multi-tendon systems [35]. More specifically, the idea that there is an agonist tendon that produces torque in the desired sense, which is opposed by an antagonist tendon on the "other side" of the joint does not extrapolate well. In the case of two or more kinematics degrees of freedom, each tendon produces a specific combination of joint torques; and all constitute a basis for mechanical actions. The positive addition of their actions (muscles can only pull, not push) creates the set of feasible outputs; be they in the joint torque space (feasible torque set) or the end-point space (feasible wrench set). Thus the routing of each tendon and the strength of each muscle can dramatically affect the size and shape of the feasible actions of the system. In the multi-joint case, therefore, mechanical actions are a vector addition of these basis vectors, and it is no longer possible to label some muscles as agonists or antagonists. This is because all active basis vectors contribute to the task equally. That is, the loss of any one muscle will affect the ability to implement that solution. Similarly, the vector addition of all contributing vectors at times requires the simultaneous cancellation of mechanical actions at a joint [34]. This can lead to activity in muscles on opposite sides of a joint, which has often been called co-contaction by extrapolation from the single joint case. However, such simultaneous activity is not optional strategy in the sense that co-contraction is usually thought of. Rather, such vector addition that engages muscles on either side of a joint is at times simply what is required to accomplish the task [38] and is not a always a decision the nervous system makes to, for example, increase joint impedance, etc.
- *Muscle Redundancy and Synergies*: More recently we have called attention to the fact that muscle redundancy, while mathematically undeniable, does not necessarily imply robustness to muscle dysfunction [39]. That is, the solution space for a given task has a specific structure given by the constraints of the task [34]. This structure then defines which muscles must be active at a level higher than zero (and are therefore necessary); and which muscles are needed at moderate or high levels of activation (and therefore the task is sensitive to weakness or dysfunction of those muscles) [39]. Lastly, because the structure of the solution space is given by the interaction among the topology of the plant and the constraints of the task, it is not surprising (in fact, it is expected) that EMG and other recordings often exhibit a lower dimensional structure [40]. This structure depends directly on how many tendons there are, how they are routed, how they can be used to fulfill the constraints of the task and is not necessarily the consequence of a specific choice of neural control strategy. Disambiguating mechanically necessary vs. neurally optional features of muscle coordination required using the techniques presented here to identify the solution space for a task given a specific tendon topology.

Therefore, our work here is motivated by the need to be able to test the functional and control consequences of any topology for a tendon-driven systems, be it biological or mechatronic. Moreover, the predictions and interpretations mentioned above depend to a certain extent on the validity of such linear methods to find and describe the structure of the solution space for static force production. Therefore, it is of critical interest to be able to validate these methodology predictions experimentally.

IV. Finger Construction

We had several design requirements when designing a reconfigurable robotic finger as a test bed for analysis, optimization, and testing. They were

1) Ability to arbitrarily change tendon routing (i.e., the joints each tendon crosses, and whether they produce positive or negative torque at each joint).
2) Ability to vary pulley sizes (i.e., moment arms of the tendons)
3) Low friction
4) Sufficient and well arranged degrees-of-freedom (DOFs) to allow three-dimensional endpoint motion and force production
5) Robust, durable, rigid

We designed the finger in SolidWorks 2010 (Dassault Systémes), as shown in Figure 1. The actual reconfigurable finger is also shown. It was constructed with one ad-abduction DOF and two flexion-extension DOFs. The primary materials were aluminum (for the links and terminating pulleys), turcite (for the spacers and rotating pulleys), and ball bearings with extended inner rings (mounted on all pulleys and link axes). All of the pulleys were custom-machined and two sizes were constructed for reconfigurability: a radius of 8.0mm for the large pulleys and 4.4mm

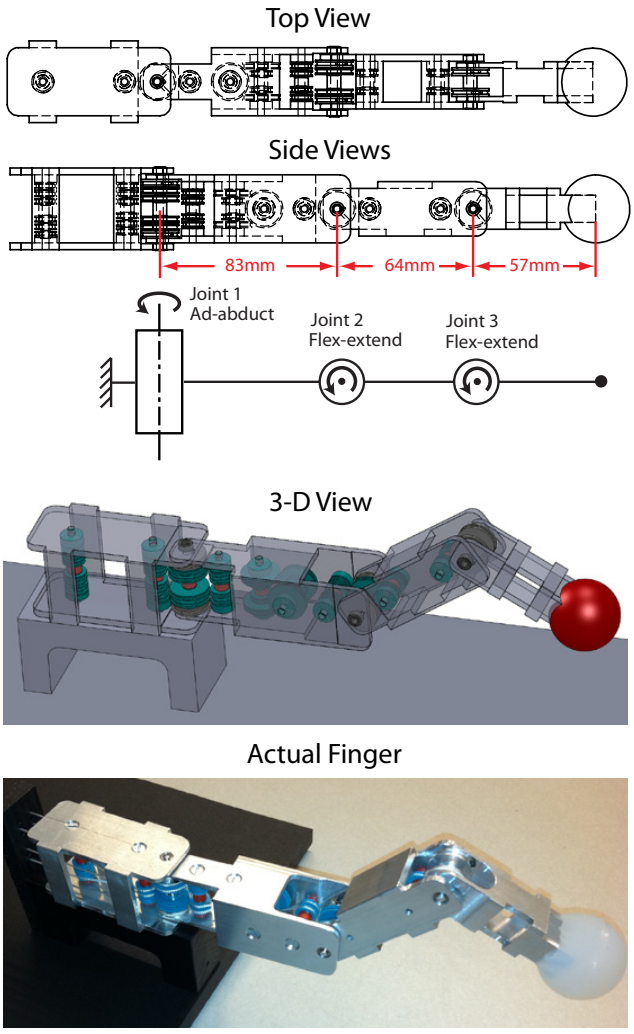

Fig. 1. 2-D and 3-D views of finger model in SolidWorks, and the actual finger.

for the small pulley, as shown in Figure 2. There were multiple pulleys that had to be added between the axes to ensure reconfigurability of the tendon routing (i.e., that each tendon could rout on either side of every joint and no bowstringing of the tendons would occur).

The selection of link lengths and pulley sizes was otherwise fairly arbitrary, and since our study did not involve optimization of incremental changes in these parameters (except the 2 pulley sizes), we simply constructed it to have reasonable size that could be fabricated and tested.

V. Methods

After construction of the finger with the desired capabilities, we were then able to analyze and optimize tendon routing and pulley sizes based on the actual kinematics and reconfiguration options of the finger.

A. Force polytope analysis

Quantification of the force-production capabilities of a robotic finger (or manipulator) can be accomplished by determination of the feasible force set (or force polytope) of the finger. This convex set encloses all feasible forces that the fingertip can exert given kinematic parameters, tendon routing and pulley sizes, and maximal tendon tensions. A quality metric that can be assigned to this set is known as the maximal isotropic value (MIV) [18]. Since we are not assuming any specific task that this finger must perform, then we chose to use this metric. We could have used any other metric instead of the MIV. Further comments can be found in the discussion section.

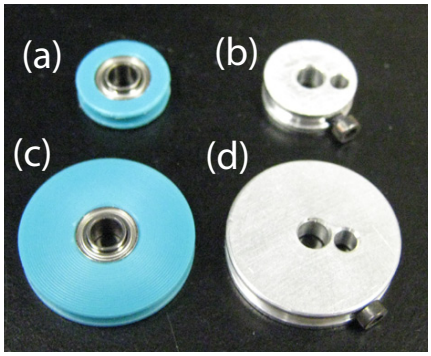

Fig. 2. Pulleys used in finger design. (a) Turcite rotating small pulley. (b) Aluminum terminating small pulley. (c) Turcite rotating large pulley. (d) Aluminum terminating large pulley.

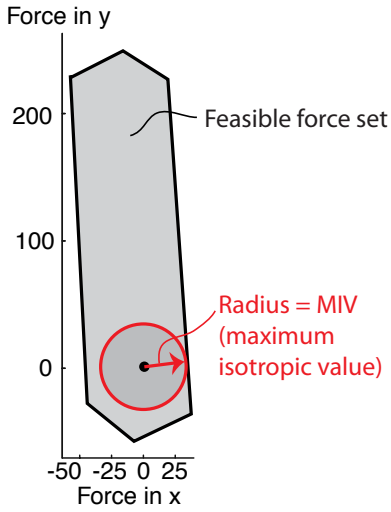

Fig. 3. Illustration of calculation of MIV (maximum isotropic value) from feasible force set.

The MIV is the radius of the largest ball, centered at the origin, that the feasible force set can contain, as illustrated in Figure 3 for a 2-D feasible force set. A finger can exert at least that many units of force in any direction.

We can use an activation vector, $\vec{a}$, to represent the degree to which a tendon is activated. Each element of $\vec{a}$ ranges between 0 (no activation, zero force) and 1 (full activation, maximal force). Further discussion may be found in [35]. If we define F_0 as a diagonal matrix of maximal tendon tensions, R as the moment arm matrix (or structure matrix) relating tendon tensions to joint torques, and J as the posture-dependent Jacobian relating joint velocities to fingertip velocities, then we can get the fingertip force vector $\vec{f}$ from tendon activations [34] if the Jacobian is square and invertible:

$$\vec{f} = J^{-T} R F_0 \vec{a} = A\vec{a} \tag{1}$$

For a given fixed finger posture, the J^{-T}, R, and F_0 matrices can be grouped into a linear mapping from activations into fingertip force, which we call an action matrix A [34], [35]. Each column of A represents the force vector each tendon produces at the fingertip in that posture if fully activated. The collection of all such forces (i.e., all columns of matrix A) forms a set of output force basis vectors. Linearity of this mapping holds true for static forces because the Jacobian and moment arms remain constant. The Minkowski sum of these basis vectors forms the feasible force set of the fingertip, and can be computed by taking the convex hull of the points generated by mapping each vertex of the activation hypercube (i.e., each vertex of the unit hypercube in the positive orthant) to fingertip wrench space via the action matrix A [34].

There are two ways to describe a convex hull: i) a set of vertices and ii) a set of linear inequalities. Vertex enumeration methodologies can calculate one description given the other. The Qhull software package uses the

Quickhull algorithm [41] and is used to perform the MIV calculations in this study. Other vertex enumeration algorithms that can perform these calculations easily include CDD [42] and LRS [43].

The description involving a set of linear inequalities (similar to a linear programming inequality constraint formulation) takes the form

$$Ax \leq b \tag{2}$$

where A is a matrix of constants defining the inequalities, x is a vector of variables of length d, where d is the dimensionality of the convex hull, and b is a vector of constants. If we denote A_i as the i^{th} row of A, then the linear inequality $A_i\mathbf{x} \leq b_i$ defines a halfspace, which also defines a facet of the convex hull. The perpendicular (i.e., shortest) Euclidean distance (or offset) of this facet from the origin, in general, will be given by

$$\frac{b_i}{\|A_i\|_2} \tag{3}$$

The Qhull output, however, automatically sets each $\|A_i\|_2$ equal to 1, so the i^{th} offset from the origin is simply the signed constant b_i. Calculation of the MIV in this study involves simply finding the minimum of b corresponding to the feasible force set.

For our finger, the Jacobian is a 3×3 matrix which is square and invertible in our experimental postures, R is a $3 \times \ell$ matrix (ℓ is the number of tendons, which is 4, 5, or 6), and F_0 is an $\ell \times \ell$ diagonal matrix of maximal tendon tensions.

B. Evaluating tendon routings

The construction of the finger allowed for various moment arm matrices to be implemented which had 4, 5, or 6 tendons. These designs are known as N+1, N+2, and 2N designs, where N is the degrees of freedom of the finger. We enumerated all possible moment arm matrices beginning with the "base" matrices shown in Figure 4. The N+2a and N+2b designs differ only in that the second tendon terminates at the first joint in the N+2a designs and at the second joint in the N+2b designs. We replaced each '#' with either a 1 or -1 (in accordance with the sign of the moment exerted on a joint when the corresponding tendon is under tension; see Figure 1 for definition of joint axes) in a full combinatoric search and then checked the controllability (i.e., that all of the joints could be actuated independently in torque and motion) conditions as described in [22]. We then calculated the MIV for these routings using the large pulleys in the main posture: 0° at joint 1, -45° at joint 2, and -45° at joint 3, as shown in Figure 5. To make comparisons feasible across finger designs with different number of tendons, we used a uniform maximal tendon tension distribution, with the sum being constrained[1] to 60N (i.e., for designs with 4, 5, and 6 tendons, the maximal tensions were 15N, 12N, and 10N, respectively). We found that many of the admissible routings produced the exact same MIVs and feasible force set volumes, likely corresponding with structurally isomorphic routings [22]. The number of routings that produced unique MIVs was a very small subset of the admissible routings, as can be seen from the numbers in Figure 4. In cases of optimization of a more complex finger or manipulator where the number of unique MIVs may be orders of magnitude higher, methods for selection of a subset for further optimization such as in [46] may be used.

The total number of routings producing distinct feasible force sets[2] was 40. For each of those routings, we calculated the MIV for all combinations of large and small pulleys. For example, the N+1 design has 9 moment

[1]The sum of maximal tendon tensions being equal is an important constraint due to the size, weight, and motor torque (and therefore tendon tension) limitations inherent in dexterous hands. For example, the torque capacity of motors is roughly proportional to motor weight, and minimization of weight was an important consideration in the design of the DLR Hand II [44]. In addition, the maximal force production capabilities of McKibben-style muscles are roughly proportional to cross- sectional area [45]. Since the actuators typically will be located in the forearm, then the total cross-sectional area will be limited to the forearm cross-sectional area. In this study, for simplicity and without affecting the generalizability of our approach or results, we do not consider alternative constraints on the actuation system (e.g., electrical current capacity, tendon velocities, etc).

[2]Due to the nature of our full combinatoric search, moment arm matrices that produced mirrored feasible force sets about a plane passing through the origin (which would have the same MIV) were discarded and also those moment arm matrices that were produced by a rearrangement of the columns. For example, in Figure 4, interchanging columns 5 and 6 does not change the feasible force set, it only reverses the "numbering" of the tendons. But in the full combinatoric search, both of these numberings would be different matrices producing identical feasible force sets.

N+1 design:
24 admissible,
3 unique

$$R = \begin{bmatrix} \# & \# & \# & \# \\ 0 & \# & \# & \# \\ 0 & 0 & \# & \# \end{bmatrix}$$

N+2a design:
88 admissible,
6 unique

$$R = \begin{bmatrix} \# & \# & \# & \# & \# \\ 0 & 0 & \# & \# & \# \\ 0 & 0 & 0 & \# & \# \end{bmatrix}$$

N+2b design:
296 admissible,
11 unique

$$R = \begin{bmatrix} \# & \# & \# & \# & \# \\ 0 & \# & \# & \# & \# \\ 0 & 0 & 0 & \# & \# \end{bmatrix}$$

2N design:
872 admissible,
20 unique

$$R = \begin{bmatrix} \# & \# & \# & \# & \# & \# \\ 0 & 0 & \# & \# & \# & \# \\ 0 & 0 & 0 & 0 & \# & \# \end{bmatrix}$$

Fig. 4. Base moment arm matrices used when finding admissible and unique tendon routings.

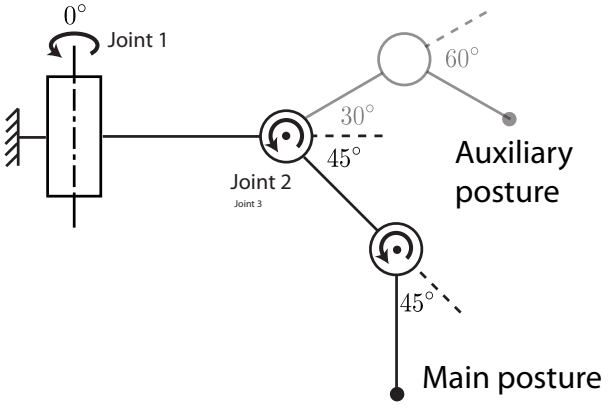

Fig. 5. Finger posture used in computations and experimental testing.

arm values. Therefore, there are 2^9 combinations of large and small pulleys for that case. Taking the combination with the highest MIV for each routing gave 40 moment-arm-optimized routings. Therefore, we had 40 unoptimized routings and 40 optimized routings. Out of these 80, we chose 6 different routings to test experimentally in a fashion that permitted testing of a large range of MIVs, and included the design with the highest predicted MIV. Otherwise the selection was arbitrary.

C. Experimental testing of tendon routings

For each of the tendon routings tested, we first arranged the pulleys and strings (0.4mm braided polyester twine) to match the desired configuration. We then mounted the finger onto a base that was part of a motor array system as shown in Figure 6. The DC motors were coupled to capstans on which the string wound. Each string was then routed around pulleys that were attached to load cells (Interface SML 25, Scottsdale, AZ) which provided force measurements for the closed-loop controller implemented in Realtime LabView. The endpoint of the finger was fixed to a custom made gimbal which constrained translational motion but not rotational motion (we did not want the fingertip to be over-constrained). The gimbal was attached to a 6-axis load cell (JR3, Woodland, CA). The sampling rate and control loop frequency were both 100Hz.

A small pretension of 1N was applied to each string to remove slack and prevent it from falling off of the pulleys. Then each vertex of the activation hypercube (as described in the previous section) was applied to the strings (in addition to the pretension) in ramp-up, hold, and ramp-down phases to find the feasible force set [39]. As in prior work, [39], vertices of this experimental feasible force set were determined from the hold phases and then used to find the MIV using Qhull as described earlier. The experimental MIV could then be compared with the theoretical MIV (from computational results).

To compare the shapes of the experimental and theoretical feasible force sets, we first normalized the volume of the experimental feasible force set to make it equal to the volume of the theoretical feasible force set. We then

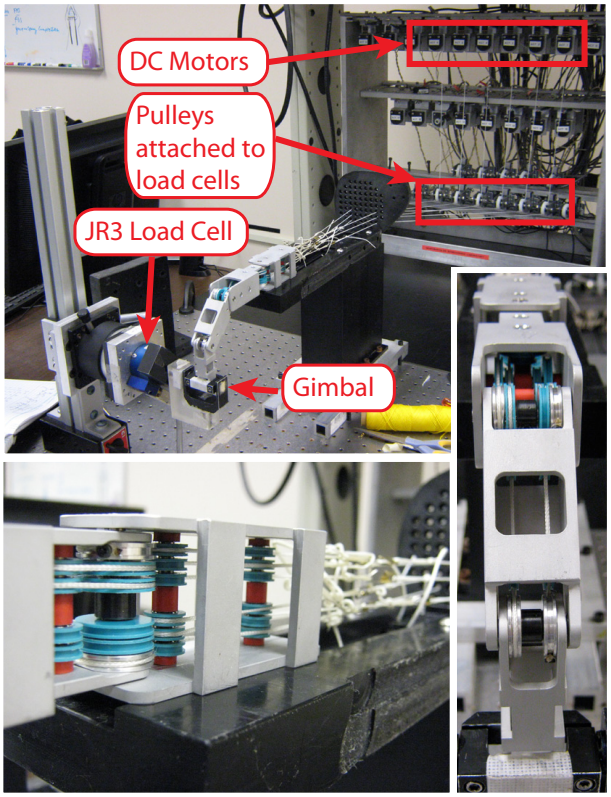

Fig. 6. Experimental system for feasible force set testing.

calculated the mean Euclidean distance of each vertex from the theoretical feasible force set from the corresponding vertex in the experimental feasible force set. We did this because there was always friction loss in the experiment[3]. In addition, we calculated the average angle between the two vectors (starting and the origin and ending at the corresponding vertex) formed from corresponding vertices.

We tested the finger in the main posture (for which we optimized MIV) and an auxiliary posture (to validate the predictions more fully). These postures are shown in Figure 5. For each design and posture, we did three repetitions of tests. Since there were 6 designs, 2 postures, and 3 repetitions, we conducted a total of 36 tests.

VI. Results

A. Calculating maximum isotropic values

The 40 unique unoptimized and 40 unique optimized routings produced the MIVs shown in Figures 7a and b. Optimization of the pulley sizes increased the average MIV from 0.60N to 0.78N, a 30% increase as shown in Figure 7a, and the maximum increase for a routing by this optimization was 82%. It is interesting to note that this force-production capability increase is achieved by simply decreasing specific pulley sizes in an informed manner. We can see from Figure 7b that designs with 4 tendons could not produce MIVs higher than the best designs with 5 or 6 tendons. However, the best design with 4 tendons did have a higher MIV than many alternative routings that had more tendons. In addition, the maximal increase from only rerouting tendons (no pulley size optimization) was 277% (i.e., the increase from the worst admissible routing to the best admissible routing for a given number of tendons).

[3]Take an extreme case in which friction loss was 50% exactly for every tendon. The theoretical feasible force set is a unit cube. While the shape of the experimental feasible force set would be also an exact cube, it would be 50% contracted in every direction and therefore the corresponding vertices would be far from each other. If we normalized the volume, the corresponding vertices would be in the same location, and the mean distance (in shape similarity) would be zero.

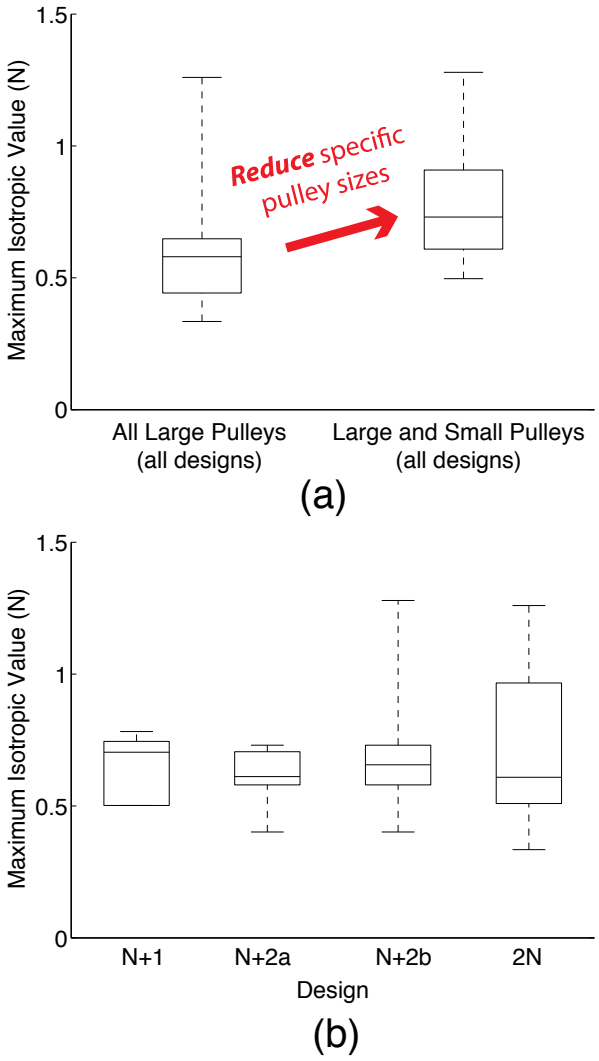

Fig. 7. Maximum isotropic values for various routings. (a) Boxplot of MIV for all designs before and after pulley-size optimization. (b) Boxplot of MIV vs. design (includes optimized and unoptimized pulley sizes).

B. Theoretical predictions vs. experimental results

The experimental results and the routings tested are shown in Figure 8. The data points shown in Figure 8b are averages of the three test repetitions in both the main posture and the auxiliary posture for each of the designs. The average standard deviation from the three test repetitions was very low at 0.0090N, showing that the results for each design/posture combination were extremely repeatable. We see a consistent linear relationship between theoretical and experimental MIVs with an R^2 value of 0.987. This result shows that the theoretical calculations are very good at predicting actual performance. The slope of the line is 0.879, which we interpret to represent an average loss of performance of about 12% from theoretical predictions, likely due mainly to friction in the system. We show experimental and theoretical feasible force sets for one test of designs 1 and 6 in the main posture in Figure 8d, and we can see visually that the shape of the theoretical feasible force sets was extremely similar to those of the experimental feasible force sets, although the experimental ones were contracted to an extent.

We can see several interesting features in Figure 8. First of all, in Figure 8a, we see that routings 1 and 5 are identical except that 2 of the signs in the moment arm matrix are reversed (i.e., 2 of the tendons are switched from one side of the ad-abduction joint to the other). However, we can see in Figure 8b and the table in Figure 8c that the MIV of routing 5 is more than twice that of routing 1 both theoretically and experimentally. Figure 9 emphasizes this large change in MIV for a small, intelligent (but perhaps counterintuitive before performing the analyses) change in tendon routing. Secondly, the MIVs of routings 5 and 6 are very similar, but routing 6 has

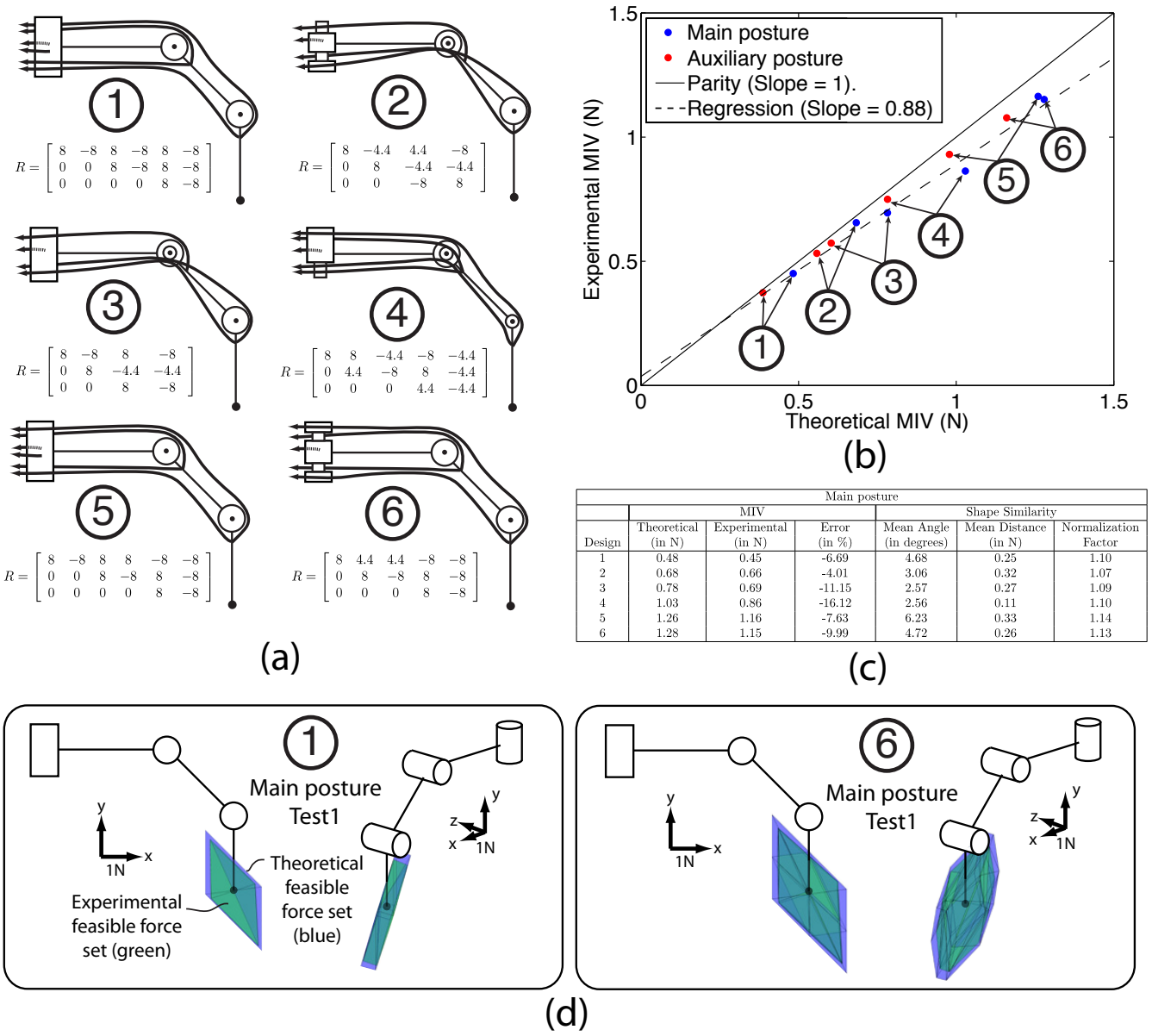

Main posture						
	MIV			Shape Similarity		
Design	Theoretical (in N)	Experimental (in N)	Error (in %)	Mean Angle (in degrees)	Mean Distance (in N)	Normalization Factor
1	0.48	0.45	-6.69	4.68	0.25	1.10
2	0.68	0.66	-4.01	3.06	0.32	1.07
3	0.78	0.69	-11.15	2.57	0.27	1.09
4	1.03	0.86	-16.12	2.56	0.11	1.10
5	1.26	1.16	-7.63	6.23	0.33	1.14
6	1.28	1.15	-9.99	4.72	0.26	1.13

Fig. 8. Results from experimental testing of various routings. (a) The 6 different routings tested. Shown to scale. R matrix values are in mm. (b) Experimental vs. theoretical MIV. Parity line is where experimental MIV would be exactly equal to theoretical MIV (intercept of 0, slope of 1). Regression has an R^2 value of 0.987. (c) Table of averages from 3 tests for each design in main posture. (d) 3-D visualization of experimental and theoretical feasible force sets for designs 1 and 6.

one less tendon. Thirdly, routings 2 and 3 have two fewer tendons than routing 1 but still outperform it in terms of MIV. Figure 8d demonstrates visually that the experimental feasible force sets corresponded very closely with the theoretical feasible force sets in shape, and that the size was similar but contracted by a small amount due to friction. While the side views of both of these feasible force sets look similar, the isometric views show clearly that the feasible force set of routing 1 is quite thin along one direction (which results in a low MIV) and the feasible force set of routing 6 is much more expanded in all directions (so the MIV is much higher).

In Figure 8b, we see that the data points lie underneath but fairly close to the parity line (if the theoretical and experimental MIVs were identical, the data points would lie exactly on the parity line). As would be expected, none of them are above the parity line. In the table in Figure 8c, we see that the error in the prediction of MIV ranged roughly between 4% and 16% which is the percentage MIV below the parity line where the data points are located. As far as shape goes, we see that the average difference in angles between corresponding vertices of the feasible force sets was between 2.56° and 6.5°. A small amount of angular error would be expected due to

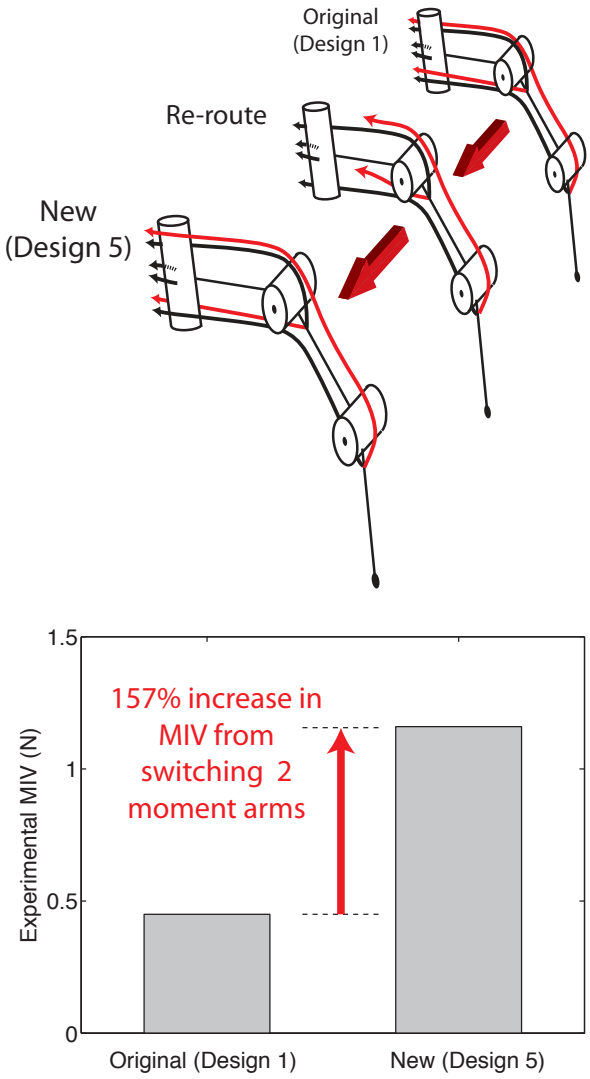

Fig. 9. Illustration of a simple (but intelligent) tendon re-routing that drastically increases MIV.

error in the positioning and alignment of the JR3 axes relative to the finger axes, so this contributes to the average difference in angles. The mean distance of corresponding vertices is less than 0.35N. The normalization factors were less than 1.15, and it is the factor by which the experimental feasible force set had to be expanded in every direction to have the same volume as the theoretical feasible force set. It roughly corresponds with the MIV error.

VII. Discussion

In this work, we have investigated the effect of various tendon routings on the set of feasible forces that can be exerted by a robotic finger both computationally and in a physical system. We see that routing has a very dramatic effect on the shape and size of the feasible force set. We also see that computational predictions are quite accurate and that they can be useful when making informed design decisions. Therefore the main conclusions of this study are twofold:

1) Different routings in robotic fingers can result in extremely different force-production capabilities.
2) Theoretical feasible force set analyses predict experimental force-production performance quite well and therefore they are a useful design tool.

One application of this work is to design tendon-driven fingers and manipulators for a given task that are optimized in terms of minimal size, weight, complexity, and cost. Since tendon-driven systems are linear for fixed postures, if we double all the moment arms (or the maximal tensions of all tendons), we double the size of feasible force set

in every direction. Our results showed that the MIV for routing 6 was more than 100% greater than that of routing 1. Therefore, one could either reduce all of the maximal tendon tensions or all of the moment arms in routing 6 by 50% and still have a greater MIV than routing 1. In a robotic hand system, if the maximal tendon tensions were cut in half (by implementing smaller motors), then the weight of the actuators could be roughly halved and cost would be reduced. This would be very desirable, in general. If tendons are driving a minimally-invasive surgical instrument, then the moment arms could be halved and therefore the diameter of the instrument would be halved (which actually would reduce the cross-sectional area by 75%!). The instrument would then be much smaller and could be much better suited for certain surgical procedures.

We have used MIV as the fitness metric for our analyses since no prior assumption of task specification was made. We acknowledge that in general, the MIV would typically be more practically used for a tendon-driven, multi-purpose manipulator rather than a robotic finger. These analyses and optimizations that we described apply equally to tendon-driven manipulators and fingers regardless of size. Since we were only testing one finger in this paper, we decided to use the MIV. Current work has accomplished design optimization and validation for grasp quality of multiple fingers of identical design to the one in this paper [47] .

If a necessary task or set of tasks is known (e.g., to have high flexion force for strong grasps) then the analyses could assign a fitness metric to a routing based on that task specification. The optimization could then be based on that metric. For example, if it is desired to have a very strong flexion force with low extension force requirements, then linear programming can easily be used to determine the maximal force possible in the flexing direction(s) after the feasible force set has been calculated (e.g., using the generic procedure outlined in [24]). We have previously described that the feasible force sets of the human fingers are asymmetrically biased towards endpoint forces in the flexion direction than in the extension which is anatomically reasonable for grasping tasks [34], [48]–[50]. If strong grasp and minimal size/weight/cost is desired for a set of fingers, then analyses like those used in [51] can be used to design an optimized tendon-driven robotic hand.

We have investigated force-production capabilities in this paper, but there are many other considerations that go into the design of a robotic hand. Other significant considerations include the robustness and effectiveness of control algorithms, passive stiffness characteristics, sensitivity to friction and positioning errors, and maximal endpoint velocities. We acknowledge that force-production capabilities are only one piece of the design puzzle for optimized robotic fingers.

For reasons of practicality, we only analyzed and constructed routings where the tendons routed around every joint that they passed (i.e., that the structure matrix is pseudo-triangular, as in [22]) and where there were only two sizes of pulleys that could be chosen. Routings can, however, be designed where tendons pass through the center of joints [52], or where moment arms can have many feasible magnitudes. This opens up the design space even more, and exhaustive searches like the ones we performed in this study may be more laborious, or even not be feasible given the exponential growth of design options. In addition, tendon-driven fingers or manipulators with more than 3 degrees of freedom will tend to suffer from the curse of dimensionality in the design space, and a designer may have to use various optimization algorithms [1] in a search for a "good enough" design which could then be selected for physical construction. Alternatively, a designer could come up with a handful of feasible, physically-realizable routings and then search in the vicinity of that region of the parameter space to determine feasible improvements with affordable computational cost [53].

The optimization process we used in this study only addressed this realization of a robotic finger. If a general robotic finger or manipulator has more joints or tendons, the dimensionality of the design space increases dramatically and finding a globally optimum solution for a specific fitness metric (of which any task-specific metric may be used, not only the general MIV metric) may be computationally infeasible due to the curse of dimensionality. Other custom or typical optimization algorithms could be used to find solutions with a high fitness. Furthermore, in the case when the optimization may involve link lengths and D-H parameters in addition to tendon routing, number of tendons, and pulley sizes, then finding a locally optimal solution or just a good-enough solution could still be very useful. The main purpose of this study was to investigate the correlation of predictions with experiments, as opposed to identifying a general optimization method for tendon-driven robotic fingers and manipulators.

Tendon friction was a significant factor in our experiment, (as it is for any tendon driven system), especially for the tendons at the last joint that had to wrap around as many as 12 pulleys. The main source of friction seemed to be the pulleys, as general observation of the data indicated that tendons attached to the ad-abduction joint (which wrapped around 4 pulleys) suffered from very little friction loss (less than a few %) while the tendons that attached

to the last joint (which wrapped around 12 pulleys and routed through the fairly complicated tendon redirection between the first and second joints) suffered from as much as 20% friction loss.

Future work will extend this experimental validation approach to routings of multiple fingers for optimized grasp quality. In addition, this work is easily applicable to refine the design of generic tendon-driven manipulators. Furthermore, investigation of the control and structure of biological tendon-driven systems is now made possible using a similar framework.

VIII. Conclusions

We conclude from this validation that these computational methods are effective at predicting the performance of drastically different tendon-driven robotic finger (or manipulator) designs, and are therefore a useful design tool. Various benefits of fully utilizing this design tool include

1) Minimization of weight: if a superior design has a force-production performance twice that of an inferior design, the superior design's actuators only need to be half the strength of the inferior design's to match the inferior design's performance, which in general corresponds to a large reduction in weight of the actuators.
2) Minimization of size: if a superior design has a force-production performance twice that of an inferior design, the superior design's moment arms only need to be half the size of the inferior design's to match the inferior design's performance, which could be used to half the overall thickness of the finger (or manipulator, or minimally-invasive surgical device).
3) Minimization of number of tendons (and therefore actuators): If a design with less tendons (such as an N+1 design) can be synthesized with the same force-production performance as that of one with more tendons (such as a 2N design), then the actuator system can be simplified and less space to rout the tendons inside the finger (or manipulator, or minimally-invasive surgical device) is needed.

Acknowledgment

The authors gratefully acknowledge the help of Dr. Manish Kurse in providing the data acquisition routine for the experimental procedure, and Dr. Veronica Santos for construction of the gimbal used in the experiments.

References

[1] J. M. Inouye, J. J. Kutch, and F. J. Valero-Cuevas, "A novel synthesis of computational approaches enables optimization of grasp quality of tendon-driven hands," *Accepted February 2012 to IEEE Transactions on Robotics*.

[2] S. Jacobsen, E. Iversen, D. Knutti, R. Johnson, and K. Biggers, "Design of the utah/mit dextrous hand," 1986, pp. 1520–1532, 1986 IEEE International Conference on Robotics and Automation. Proceedings.

[3] J. K. Salisbury and J. J. Craig, "Articulated hands: Force control and kinematic issues," *The International Journal of Robotics Research*, vol. 1, no. 1, p. 4, 1982.

[4] Shadow Dexterous Hand, Shadow Robot Company.

[5] M. Grebenstein, A. Albu-Schffer, T. Bahls, M. Chalon, O. Eiberger, W. Friedl, R. Gruber, U. Hagn, R. Haslinger, and H. Hppner, "The dlr hand arm system," *Submitted to ICRA*, vol. 11.

[6] R. O. Ambrose, H. Aldridge, R. S. Askew, R. R. Burridge, W. Bluethmann, M. Diftler, C. Lovchik, D. Magruder, and F. Rehnmark, "Robonaut: Nasa's space humanoid," *IEEE Intelligent Systems and Their Applications*, vol. 15, no. 4, pp. 57–63, 2000.

[7] B. M. Jau, "Dexterous telemanipulation with four fingered hand system," vol. 1. IEEE, 1995, pp. 338–343 vol. 1, robotics and Automation, 1995. Proceedings., 1995 IEEE International Conference on.

[8] B. Massa, S. Roccella, M. C. Carrozza, and P. Dario, "Design and development of an underactuated prosthetic hand," vol. 4. IEEE, 2002, pp. 3374–3379 vol. 4, robotics and Automation, 2002. Proceedings. ICRA'02. IEEE International Conference on.

[9] L. R. Lin and H. P. Huang, "Mechanism design of a new multifingered robot hand," vol. 2. IEEE, 1996, pp. 1471–1476 vol. 2, robotics and Automation, 1996. Proceedings., 1996 IEEE International Conference on.

[10] H. Kawasaki, T. Komatsu, and K. Uchiyama, "Dexterous anthropomorphic robot hand with distributed tactile sensor: Gifu hand ii," *Mechatronics, IEEE/ASME Transactions on*, vol. 7, no. 3, pp. 296–303, 2002.

[11] A. Namiki, Y. Imai, M. Ishikawa, and M. Kaneko, "Development of a high-speed multifingered hand system and its application to catching," vol. 3. IEEE, 2003, pp. 2666–2671 vol. 3, intelligent Robots and Systems, 2003.(IROS 2003). Proceedings. 2003 IEEE/RSJ International Conference on.

[12] I. Yamano and T. Maeno, "Five-fingered robot hand using ultrasonic motors and elastic elements." IEEE, 2005, pp. 2673–2678, robotics and Automation, 2005. ICRA 2005. Proceedings of the 2005 IEEE International Conference on.

[13] I. Gaiser, S. Schulz, A. Kargov, H. Klosek, A. Bierbaum, C. Pylatiuk, R. Oberle, T. Werner, T. Asfour, and G. Bretthauer, "A new anthropomorphic robotic hand." IEEE, 2008, pp. 418–422, humanoid Robots, 2008. Humanoids 2008. 8th IEEE-RAS International Conference on.

[14] J. L. Pons, R. Ceres, and F. Pfeiffer, "Multifingered dextrous robotics hand design and control: a review," *Robotica*, vol. 17, no. 6, p. 674, 1999.

[15] F. Firmani, A. Zibil, S. B. Nokleby, and R. P. Podhorodeski, "Wrench capabilities of planar parallel manipulators. part i: Wrench polytopes and performance indices," *Robotica*, vol. 26, no. 06, pp. 791–802, 2008.

[16] S. Bouchard, C. M. Gosselin, and B. Moore, "On the ability of a cable-driven robot to generate a prescribed set of wrenches." Citeseer, proc. of the ASME International Design Engineering Technical Conferences, Mechanics and Robotics Conference, 2008.

[17] P. Chiacchio, Y. Bouffard-Vercelli, and F. Pierrot, "Force polytope and force ellipsoid for redundant manipulators," *Journal of Robotic Systems*, vol. 14, no. 8, pp. 613–620, 1997.

[18] R. Finotello, T. Grasso, G. Rossi, and A. Terribile, "Computation of kinetostatic performances of robot manipulators with polytopes," vol. 4. IEEE, 1998, pp. 3241–3246, robotics and Automation, 1998. Proceedings. 1998 IEEE International Conference on.

[19] M. Gouttefarde and S. Krut, "Characterization of parallel manipulator available wrench set facets," *Advances in Robot Kinematics: Motion in Man and Machine*, pp. 475–482, 2010.

[20] A. Zibil, F. Firmani, S. B. Nokleby, and R. P. Podhorodeski, "An explicit method for determining the force-moment capabilities of redundantly actuated planar parallel manipulators," *Journal of mechanical design*, vol. 129, p. 1046, 2007.

[21] L. W. Tsai, "Design of tendon-driven manipulators," *Journal of mechanical design*, vol. 117, p. 80, 1995.

[22] J. J. Lee and L. W. Tsai, "The structural synthesis of tendon-driven manipulators having a pseudotriangular structure matrix," *The International Journal of Robotics Research*, vol. 10, no. 3, p. 255, 1991.

[23] J. J. Lee, "Tendon-driven manipulators: Analysis, synthesis, and control." *PhD Dissertation, University of Maryland.*, 1991.

[24] J. L. Fu and N. S. Pollard, "On the importance of asymmetries in grasp quality metrics for tendon driven hands," 2006, pp. 1068–1075, 2006 IEEE/RSJ International Conference on Intelligent Robots and Systems.

[25] D. Z. Chen, J. C. Su, and K. L. Yao, "A decomposition approach for the kinematic synthesis of tendon-driven manipulators," *Journal of Robotic Systems*, vol. 16, no. 8, pp. 433–443, 1999.

[26] Y. J. Ou and L. W. Tsai, "Kinematic synthesis of tendon-driven manipulators with isotropic transmission characteristics," *Journal of mechanical design*, vol. 115, p. 884, 1993.

[27] ——, "Isotropic design of tendon-driven manipulators," *Journal of mechanical design*, vol. 118, no. 3, pp. 360–366, 1996.

[28] J. B. Sheu, J. J. Huang, and J. J. Lee, "Kinematic synthesis of tendon-driven robotic manipulators using singular value decomposition," *Robotica*, vol. 28, no. 01, pp. 1–10, 2009.

[29] J. Angeles, "On the optimum dimensioning of robotic manipulators." McGill University, Montreal, 2004.

[30] M. M. Aref, H. D. Taghirad, and S. Barissi, "Optimal design of dexterous cable driven parallel manipulators," *International Journal of Robotics: Theory and Applications*, vol. 2, no. 4, pp. 43–51, 2009.

[31] D. Chablat and J. Angeles, "On the kinetostatic optimization of revolute-coupled planar manipulators," *Mechanism and machine theory*, vol. 37, no. 4, pp. 351–374, 2002.

[32] W. A. Khan and J. Angeles, "The kinetostatic optimization of robotic manipulators: the inverse and the direct problems," *Journal of mechanical design*, vol. 128, p. 168, 2006.

[33] L. Kuxhaus, S. S. Roach, and F. J. Valero-Cuevas, "Quantifying deficits in the 3d force capabilities of a digit caused by selective paralysis: application to the thumb with simulated low ulnar nerve palsy," *Journal of Biomechanics*, vol. 38, no. 4, pp. 725–736, 2005.

[34] F. J. Valero-Cuevas, F. E. Zajac, and C. G. Burgar, "Large index-fingertip forces are produced by subject-independent patterns of muscle excitation," *Journal of Biomechanics*, vol. 31, no. 8, pp. 693–704, 1998.

[35] F. J. Valero-Cuevas, "A mathematical approach to the mechanical capabilities of limbs and fingers," *Progress in Motor Control*, pp. 619–633, 2005.

[36] F. J. Valero-Cuevas, V. V. Anand, A. Saxena, and H. Lipson, "Beyond parameter estimation: extending biomechanical modeling by the explicit exploration of model topology," *IEEE Trans Biomed Eng*, vol. 54, pp. 1951–1964, Nov 2007.

[37] J. M. Inouye and F. J. Valero-Cuevas, "Asymmetric routings with fewer tendons can offer both flexible endpoint stiffness control and high force-production capabilities in robotic fingers," in *BioRob Rome The Fourth IEEE RAS/EMBS International Conference on Biomedical Robotics and Biomechatronics*, 2012.

[38] F. J. Valero-Cuevas, "An integrative approach to the biomechanical function and neuromuscular control of the fingers," *J Biomech*, vol. 38, pp. 673–684, Apr 2005.

[39] J. J. Kutch and F. J. Valero-Cuevas, "Muscle redundancy does not imply robustness to muscle dysfunction," *Journal of Biomechanics*, vol. 44, no. 7, pp. 1264–1270, 2011.

[40] ——, "Challenges and new approaches to proving the existence of muscle synergies of neural origin," *PLoS Comput Biol*, vol. 8, no. 5, May 2012. [Online]. Available: http://www.hubmed.org/display.cgi?uids=22570602

[41] C. B. Barber, D. P. Dobkin, and H. Huhdanpaa, "The quickhull algorithm for convex hulls," *ACM Transactions on Mathematical Software (TOMS)*, vol. 22, no. 4, pp. 469–483, 1996.

[42] K. Fukuda and A. Prodon, "Double description method revisited," *Combinatorics and Computer Science*, pp. 91–111, 1996.

[43] D. Avis, "A revised implementation of the reverse search vertex enumeration algorithm," vol. 29, 2000, pp. 177–198, in: Polytopes - Combinatorics and Computation, G. Kalai & G. Ziegler eds., Birkhauser-Verlag, DMV Seminar Band 29.

[44] J. Butterfafl, M. Grebenstein, H. Liu, and G. Hirzinger, "Dlr-hand ii: Next generation of a dextrous robot hand," vol. 1. IEEE, 2001, pp. 109–114 vol. 1, robotics and Automation, 2001. Proceedings 2001 ICRA. IEEE International Conference on.

[45] N. S. Pollard and R. C. Gilbert, "Tendon arrangement and muscle force requirements for humanlike force capabilities in a robotic finger," *environment*, vol. 17, p. 14, 2002.

[46] G. Taguchi, S. Konishi, and I. American Supplier, *Orthogonal arrays and linear graphs: tools for quality engineering*. American Supplier Institute Allen Park, MI, 1987.

[47] J. M. Inouye, "Bio-inspired tendon-driven systems: Computational analysis, optimization, and hardware implementation," Ph.D. dissertation, University of Southern California, 2012.

[48] J. M. Inouye, J. J. Kutch, and F. Valero-Cuevas, "Quantitative prediction of grasp impairment following peripheral neuropathies of the hand," *Proceedings of the 35nd Annual Meeting of the American Society of Biomechanics, Long Beach, CA, 2011.*, 2011.

[49] F. J. Valero-Cuevas, J. D. Towles, and V. R. Hentz, "Quantification of fingertip force reduction in the forefinger following simulated paralysis of extensor and intrinsic muscles," *Journal of Biomechanics*, vol. 33, no. 12, pp. 1601–1609, 2000.

[50] F. J. Valero-Cuevas and V. R. Hentz, "Releasing the a3 pulley and leaving flexor superficialis intact increases pinch force following the zancolli lasso procedures to prevent claw deformity in the intrinsic palsied finger," *Journal of Orthopaedic Research*, vol. 20, no. 5, pp. 902–909, 2002.

[51] J. M. Inouye, J. J. Kutch, and F. Valero-Cuevas, "A novel methodology to compare grasp quality: application to two dominant tendon-driven designs," *Proceedings of the 35nd Annual Meeting of the American Society of Biomechanics, Long Beach, CA, 2011.*

[52] M. Grebenstein, M. Chalon, G. Hirzinger, and R. Siegwart, "Antagonistically driven finger design for the anthropomorphic dlr hand arm system," 2010, proc. IEEE-RAS International Conference on Humanoid Robots (HUMANOIDS).

[53] F. J. Valero-Cuevas, H. Hoffmann, M. U. Kurse, J. J. Kutch, and E. A. Theodorou, "Computational models for neuromuscular function," *IEEE Reviews in Biomedical Engineering (2) October*, pp. 110–135, 2009.